Dalton Transactions

PAPER

View Article Online
View Journal | View Issue

Cite this: *Dalton Trans.*, 2017, **46**, 6417

A facile hydrothermal synthesis of carbon dots modified g-C_3N_4 for enhanced photocatalytic H_2-evolution performance†

Xuefei Wang,[a] Jingjing Cheng,[a] Huogen Yu *[a,b] and Jiaguo Yu[c]

Received 3rd March 2017,
Accepted 18th April 2017

DOI: 10.1039/c7dt00773f

rsc.li/dalton

Carbon dots (CDs)/g-C_3N_4 is a promising photocatalyst to split water for H_2 production; however, the synthesis of CDs/g-C_3N_4 is usually rigorous and involves multiple steps, which limits its practical application. In this study, a facile hydrothermal approach was developed to prepare CDs/g-C_3N_4 photocatalysts using L-ascorbic acid and g-C_3N_4 as the precursors. Upon *in situ* thermal polymerization of L-ascorbic acid on the g-C_3N_4 surface, the carbon dots were homogeneously and solidly modified on the g-C_3N_4 surface. The CDs/g-C_3N_4 photocatalysts showed higher photocatalytic performance for H_2 production than g-C_3N_4 under UV light irradiation using lactic acid as the sacrificial agent. The improved photocatalytic performance of CDs/g-C_3N_4 was mainly attributed to rapid interfacial charge transfer. After a Pt co-catalyst was loaded, the Pt-CDs/g-C_3N_4 catalyst formed exhibited a further improved photocatalytic performance for H_2 production and could even split pure water to produce H_2. Considering our present economic and facile synthetic approach for the modification of carbon dots on the surface of g-C_3N_4 photocatalysts, the as-prepared CDs/g-C_3N_4 photocatalysts will be promising for practical use in water splitting.

Introduction

Graphitic carbon nitride (g-C_3N_4), an organic semiconductor, is a promising photocatalyst to split water for H_2 production due to its fascinating physicochemical properties including strong and wide absorption of solar spectrum,[1,2] excellent thermal and chemical stability[3–5] as well as low cost and abundance.[6–8] Unfortunately, the fast recombination rate of photogenerated charge carriers results in a low photocatalytic performance, and thus hinders the practical application of g-C_3N_4.[9–13] To achieve outstanding photocatalytic performance, therefore, it is highly desirable to realize the effective separation of photogenerated charge carriers in g-C_3N_4.

Over the past few years, a lot of effective strategies have been employed to facilitate the separation of photogenerated charge carriers in g-C_3N_4 including elemental doping,[14,15] noble metal deposition,[16–18] coupling with inorganic or organic semiconductors,[19–21] as well as modification by carbonaceous nanomaterials, such as rGO, GO, carbon nanospheres, and carbon dots.[22–25] Among the above-mentioned strategies, the modification of g-C_3N_4 using carbon dots has been considered to be one of the most efficient strategies due to its exclusive advantages. Clearly, carbon dots can act as effective electron-transfer materials to transfer the photogenerated electrons in g-C_3N_4 and reduce H_2O to H_2 because of its suitable LUMO position, which is lower than the LUMO position of g-C_3N_4 but higher than the potential position of the normal hydrogen electrode (NHE) according to recent theoretical calculations.[26–28] Furthermore, they can strongly interact with g-C_3N_4 and provide active sites for high hydrogen-evolution activity due to the sp^2 character of its C–C bonds and high oxygen content.[29,30] Moreover, carbon dots are low-cost and resource-rich and can be used to construct metal-free g-C_3N_4 based photocatalysts.[31–34] Considering the above advantages, CDs-modified g-C_3N_4 is expected to be an excellent photocatalyst with good photocatalytic performance. In recent years, some synthetic approaches have been developed to prepare CDs-modified g-C_3N_4. For example, Tang *et al.*[35] synthesized a C-dots/g-C_3N_4 photocatalyst *via* the pyrolysis of EDTA, calcination of melamine, exfoliation of bulk g-C_3N_4, and hydrothermal treatment. Similarly, Liang *et al.*[36] also prepared a C-dots/g-C_3N_4 photocatalyst *via* the pyrolysis of urea,

[a]*School of Chemistry, Chemical Engineering and Life Sciences, Wuhan University of Technology, Wuhan 430070, PR China. E-mail: yuhuogen@whut.edu.cn; Fax: +86-27-87879468; Tel: +86-27-87871029*
[b]*State Key Laboratory of Silicate Materials for Architectures, Wuhan University of Technology, Wuhan 430070, PR China*
[c]*State Key Laboratory of Advanced Technology for Material Synthesis and Processing, Wuhan University of Technology, Wuhan 430070, PR China*

†Electronic supplementary information (ESI) available. See DOI: 10.1039/c7dt00773f

acid treatment of g-C_3N_4, electrochemical synthesis for CQDs, and physical mixing of C-dots and g-C_3N_4. The obtained C-dots/g-C_3N_4 photocatalysts exhibited excellent photocatalytic performance for H_2 production and the degradation of organic substrates; however, the synthetic approaches are usually complicated and the interfacial contacts between the carbon dots and g-C_3N_4 are usually weak and inhomogeneous. To realize the practical application of CDs-modified g-C_3N_4, it is highly desirable and imperative to explore the facile synthetic approaches and simultaneously realize homogeneous and solid interfacial contacts. However, to date, the successful examples are very rare due to its technical difficulty.

In this study, carbon dots were homogeneously and solidly modified on the surface of g-C_3N_4 photocatalysts using a facile and mild hydrothermal approach using L-ascorbic acid and g-C_3N_4 as the precursors. Upon the *in situ* thermal polymerization of L-ascorbic acid on the surface of g-C_3N_4, carbon dots were homogeneously and solidly modified on the surface of g-C_3N_4. It was found that the presence of carbon dots on the g-C_3N_4 surface could greatly enhance the photocatalytic activity of g-C_3N_4 for hydrogen generation using lactic acid as the sacrificial agent. The photocatalytic H_2-production performance of the CDs/g-C_3N_4 can be further enhanced with the addition of a Pt co-catalyst. Amazingly, the Pt/CDs-modified g-C_3N_4 can even split pure water to produce H_2 under UV light irradiation. A possible photocatalytic mechanism was proposed. Furthermore, the present facile hydrothermal approach used to synthesize the CDs-modified g-C_3N_4 photocatalysts can also be considered to be an effective strategy for the designing and preparation of other highly efficient photocatalysts.

Experimental

All reagents were of analytical grade, supplied by Shanghai Chemical Reagent Ltd (PR China) and used as received without further purification. Deionized water was used in all the experiments.

Synthesis of the bulk g-C_3N_4 photocatalyst

The bulk g-C_3N_4 material was synthesized using a typical high-temperature polymerization method. According to previous studies,[37] the melamine precursor was calcined at 550 °C for 4 h under ambient atmosphere to obtain the bulk g-C_3N_4, and the heating rate was kept at 5 °C min^{-1}. After cooling to room temperature, the light yellow bulk g-C_3N_4 was collected and ground into powder with an agate mortar.

Synthesis of the CDs/g-C_3N_4 photocatalysts

The CDs/g-C_3N_4 photocatalysts were directly synthesized using a facile hydrothermal method. First, L-ascorbic acid (0–0.6 g) was dissolved in deionized water (30 mL) in a 100 mL glass beaker, and ethanol (30 mL) was added to the solution to form a homogeneous solution under magnetic stirring. Subsequently, 0.6 g of the bulk g-C_3N_4 was dispersed into the abovementioned solution with magnetic stirring for 1 h and ultrasonically dispersed for 30 min. Afterwards, the mixture was transferred into a 100 mL Teflon-sealed autoclave, heated at 180 °C for 4 h and then allowed to cool to room temperature naturally. Subsequently, the as-obtained precipitates were centrifuged at 8000 rpm for 30 min and washed three times with ethanol and deionized water, sequentially, until the supernatant became colourless. Finally, the precipitates were dried in an oven at 60 °C overnight. In this case, the weight of L-ascorbic acid was controlled to be 0, 0.006, 0.03, 0.06, 0.3, and 0.6 g, and the corresponding samples were labelled as g-C_3N_4, CDs/g-C_3N_4 (1 wt%), CDs/g-C_3N_4 (5 wt%), CDs/g-C_3N_4 (10 wt%), CDs/g-C_3N_4 (50 wt%), and CDs/g-C_3N_4 (100 wt%), respectively. Furthermore, pure carbon dots were also synthesized under the same reaction conditions with L-ascorbic acid as the precursor.

Characterization

The morphology was observed using JEM-7500F field emission scanning electronic microscopy (FESEM, Hitachi, Japan). Further morphological and structural characterizations were based on transmission electron microscopy (TEM) and high-resolution transmission electron microscopy (HRTEM) observations. The TEM/HRTEM images were recorded using a JEM-2100F transmitting electron microscope. X-ray diffraction (XRD) patterns were obtained on a D/MAX-RB X-ray diffractometer (Rigaku, Japan). X-ray photoelectron spectroscopy (XPS) was carried out on a KRATOA XSAM800 XPS system with a Mg Kα radiation source. All the binding energies were referenced to the C 1s peaks at 284.8 eV of surface adventitious carbon. The Fourier transform infrared spectra (FTIR) of the samples were recorded using an IRAffinity-1 FTIR spectrometer. UV-vis absorption spectra were obtained using a UV-visible spectrophotometer (UV-2450, Shimadzu, Japan). $BaSO_4$ was used as a reflectance standard in the UV-vis diffuse reflectance experiments.

Photocatalytic H_2 production activity

The photocatalytic hydrogen-production experiments were conducted in a 100 mL three-necked Pyrex flask at ambient temperature and atmospheric pressure, and the outlets of the flask were sealed with a silicone rubber septum. Four low-power LEDs (3 W, 365 nm, Shenzhen Lamplic Science Co. Ltd) served as irradiation light sources to trigger the photocatalytic reaction, which were positioned 1 cm away from the reactor in four different directions. The focused intensity for each LED lamp on the flask was about 80 mW cm^{-2}. In a typical experiment, 50 mg of the photocatalytic powder was dispersed in 80 mL of an aqueous solution containing 8 mL of lactic acid or 80 mL pure water. The Pt co-catalyst (1 wt%) was photo-deposited on the catalysts by directly dissolving H_2PtCl_6 into the reactant suspension.[38,39] Before each experiment, the system was first bubbled with nitrogen for 30 min to remove the dissolved gas impurities. In the process of irradiation, continuous stirring was applied to keep the photocatalyst particles as a suspension. A diagram of the experimental set-up is shown in Fig. S1.† Gas (0.4 mL) was intermittently sampled through the

septum, and hydrogen was analyzed using gas chromatography system (Shimadzu GC-14C, Japan, with nitrogen as a carrier gas) equipped with a 5 Å molecular sieve column and a thermal conductivity detector. All glassware was carefully rinsed with water prior to use.

Photoelectrochemical measurements

Photoelectrochemical measurements and electrochemical impedance spectra (EIS) were carried out in a standard three-electrode configuration with a platinum wire as the counter electrode, saturated Hg/Hg_2Cl_2 (in saturated KCl) as the reference electrode, and Na_2SO_4 (0.5 M) aqueous solution as the electrolyte. The test results were recorded using an electrochemical workstation (CHI660E). The light source was provided by one 3 W LED (365 nm light source with a 80 mW cm^{-2}). A fluorine-doped tin oxide (FTO) conductor glass was used as the working electrode. Typically, the samples (10 mg) were added into 1 mL of anhydrous ethanol and 1 mL of Nafion D-520 dispersion (5% w/w, in water and 1-propanol, Alfa Aesar) and then uniformly dispersed by ultrasound to obtain a suspension. The suspension was spread on fixed 1 × 1 cm FTO glass with the side protected by Scotch tape and then dried at 60 °C overnight. A copper wire was connected to the side of the working electrode using conductive tape, and the uncoated parts of the electrode were isolated with epoxy resin. Ultimately, the transient photocurrent responses of the working electrodes with time (*i–t* curve) were measured at a 0.5 V bias potential during repeated ON/OFF illumination cycles, and the EIS was determined over the frequency range of 0.01–105 Hz with an ac amplitude of 10 mV at the open circuit voltage.

Results and discussion

The synthetic strategy used to prepare the CDs/g-C_3N_4 photocatalysts

To achieve the facile synthesis and solid interfacial contact of the CDs/g-C_3N_4 photocatalysts, the synthetic strategy used in our present study was mainly focused on the choice of the synthetic approaches and precursors used to prepare the carbon dots. Even though carbon dots can be obtained using the reported methods,[29] the subsequent physical mixing of carbon dots and g-C_3N_4 will result in a weak interfacial contact. Therefore, an optimized strategy is that the carbon dots can be modified on the surface of g-C_3N_4 using an *in situ* one-step approach, as shown in Fig. 1. First, the bulk g-C_3N_4 is synthesized *via* thermal polymerization using melamine as the precursor (Fig. 1a and b). The as-synthesized g-C_3N_4 is usually considered to be composed of the condensed tri-*s*-triazine subunits connected through planar tertiary amino groups. Furthermore, as a result of structural defects and incomplete condensation, additional amine functional groups also exist at the edge of the g-C_3N_4. Subsequently, when added to the dispersed g-C_3N_4 suspension, the L-ascorbic acid molecules are closely connected on the surface of g-C_3N_4 due to the acidic

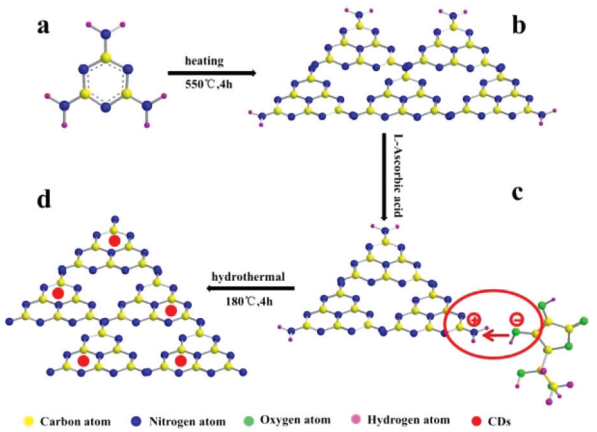

Fig. 1 A schematic of the synthesis of the CDs/g-C_3N_4: (a) melamine, (b) bulk g-C_3N_4, (c) L-ascorbic acid/bulk g-C_3N_4 complexes and (d) CDs/g-C_3N_4.

properties of the enol group in L-ascorbic acid and the alkaline properties of the amino group at the edge of the g-C_3N_4 (Fig. 1c). With the following hydrothermal treatment performed at 180 °C, the carbon dots can be formed *in situ via* the thermal polymerization of L-ascorbic acid, and thereby can be homogeneously and solidly modified on the surface of g-C_3N_4 (Fig. 1d).

The morphology and microstructures of the CDs/g-C_3N_4 photocatalysts

To verify the feasibility of our synthetic strategy, the as-prepared samples were first characterized by FESEM and TEM. From the FESEM image shown in Fig. 2a, it can be seen that the g-C_3N_4 sample shows an irregular morphology with lamellar structure due to its structural properties. Furthermore, the special lamellar structure was also ascribed to the exfoliation of bulk g-C_3N_4 and the formation of thin g-C_3N_4 nanosheets during the hydrothermal process, according to our previous report.[40] Because of the facile agglomeration of the thin g-C_3N_4 nanosheets in the sample preparation process, the g-C_3N_4 sample shows an irregular morphology. Fig. 2b–d are the FESEM images of the g-C_3N_4 samples modified with different amounts of the carbon dots, which exhibit similar morphological features with those shown in Fig. 2a, suggesting that the addition of L-ascorbic acid and the following carbonization step clearly did not destroy the structures of g-C_3N_4 in the g-C_3N_4 samples modified with different amounts of the carbon dots. However, for the CDs/g-C_3N_4 samples, the carbon dots are not visible in their FESEM images (Fig. 2b–d), possibly due to their very small particle size. As shown in the TEM image (Fig. 2f), the average size of the carbon dots, which were obtained by the hydrothermal treatment of L-ascorbic acid, consistent with a previous report, was *ca.* 5 nm.[41] In addition, Fig. 2e further shows that g-C_3N_4 has a lamellar morphology. For the CDs/g-C_3N_4 sample, it was also clearly seen that the carbon dots with an average size of *ca.* 5 nm were homogeneously dispersed on the lamellar surface of g-C_3N_4

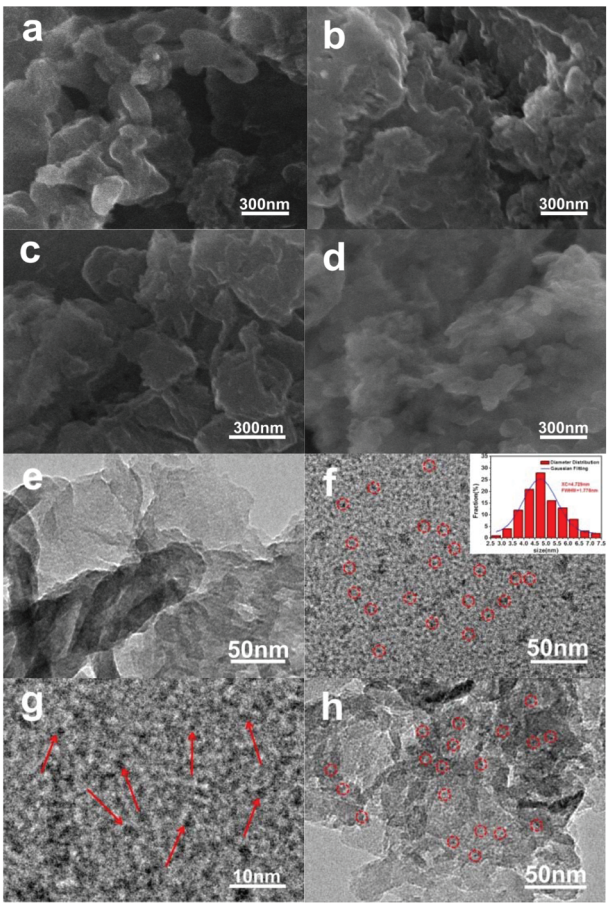

Fig. 2 FESEM images of the various samples: (a) g-C_3N_4, (b) CDs/g-C_3N_4 (5 wt%), (c) CDs/g-C_3N_4 (10 wt%) and (d) CDs/g-C_3N_4 (100 wt%). TEM images of (e) g-C_3N_4, (f and g) CDs (the inset is their diameter distribution) and (h) CDs/g-C_3N_4 (100 wt%).

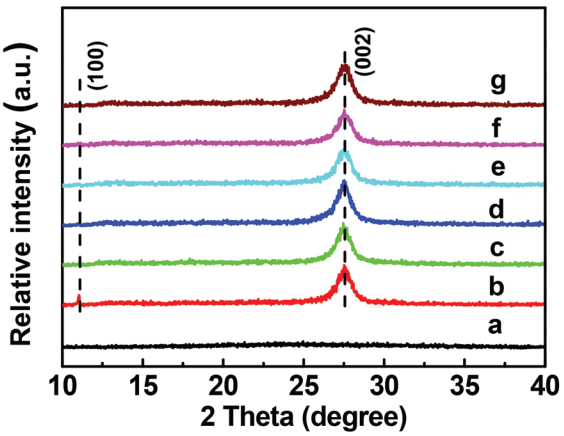

Fig. 3 XRD patterns of the various samples: (a) CDs, (b) g-C_3N_4, (c) CDs/g-C_3N_4 (1 wt%), (d) CDs/g-C_3N_4 (5 wt%), (e) CDs/g-C_3N_4 (10 wt%), (f) CDs/g-C_3N_4 (50 wt%), and (g) CDs/g-C_3N_4 (100 wt%).

(Fig. 2h). The following HRTEM image further reveals that the carbon dots have weak crystallization and are nearly amorphous (Fig. 2g). Furthermore, the EDS results and rough CDs contents of the various samples are listed in Table S1.† Clearly, the above results strongly demonstrate that the carbon dots have been homogeneously modified on the g-C_3N_4 surface to form the CDs/g-C_3N_4 photocatalyst *via* a facile hydrothermal approach.

The phase structure and composition of the as-synthesized CDs/g-C_3N_4 samples were further revealed by XRD, XPS, FTIR, and UV-vis spectra. Fig. 3 shows the XRD patterns of the various CDs/g-C_3N_4 samples. In Fig. 3a, no significant diffraction peak appears in the XRD pattern of carbon dots, which further indicates that they are nearly amorphous. For the g-C_3N_4 sample, there are two characteristic diffraction peaks positioned at 11.0° and 27.5° in Fig. 3b. According to the analysis of the previous literature,[42] the peak at 11.0° can be indexed to the (100) facet of g-C_3N_4 and is related to the in-plane structural packing of the oriented melons; the other peak at 27.5° can be indexed to the (002) facet of g-C_3N_4 and is a characteristic interplanar stacking peak of the aromatic systems. After the carbon dots were modified on the surface of g-C_3N_4, a peak at 27.5° with a similar intensity appeared in all the CDs/g-C_3N_4 samples (Fig. 3c–g), which further indicates that the modification of the carbon dots does not destroy the structure of g-C_3N_4. Nevertheless, for all the CDs/g-C_3N_4 samples, the peak at 11.0° disappeared possibly due to the strong interfacial interaction between the CDs and g-C_3N_4, which disturbs the periodic potential field of the oriented melons. The above results further suggest that the carbon dots were homogeneously and solidly modified on the surface but did not destroy the structure of g-C_3N_4.

XPS and FTIR spectroscopy were employed to further obtain the detailed chemical composition of the various samples. Fig. 4 shows the XPS spectra of the carbon dots, g-C_3N_4 and CDs/g-C_3N_4 (10 wt%). From the XPS survey spectra in Fig. 4A, it can be seen that the carbon dots are mainly composed of C and O elements, while g-C_3N_4 and CDs/g-C_3N_4 (10 wt%) mainly include the elements C, N, and O.

Even though the same elements (C and O) exist in the carbon dots and g-C_3N_4 samples, the chemical bonds formed by them are different in the samples, as shown in Fig. 4B–D. Specifically, for the carbon dots, the C 1s spectrum shows two deconvoluted peaks at 286.0 and 284.7 eV, respectively, which can be ascribed to C–OH and C–C/C=C.[43] In comparison, the C 1s spectrum of g-C_3N_4 can be deconvoluted into two peaks at 288.5 and 287.5 eV, which can be ascribed to N–C=N and C=N, respectively.[44] In addition, for the carbon dots, three deconvoluted peaks in the O 1s spectrum are positioned at 533.0, 532.1, and 531.6 eV, which were attributed to H_2O, C–O–H, and C=O, respectively.[45] However, the only peak at 531.6 eV was found for g-C_3N_4 in the O 1s spectrum. Furthermore, the chemical bond of C–N in g-C_3N_4 was further proven by the N 1s spectrum in Fig. 4C. Clearly, there are two peaks positioned at 398 and 400 eV, which are assigned to C=N–C and N–$(C)_3$ in g-C_3N_4.[5] In reference to the XPS spectra of the carbon dots and g-C_3N_4, it can be seen that CDs/g-C_3N_4 (10 wt%) shows a similar XPS spectrum with g-C_3N_4 (Fig. 4),

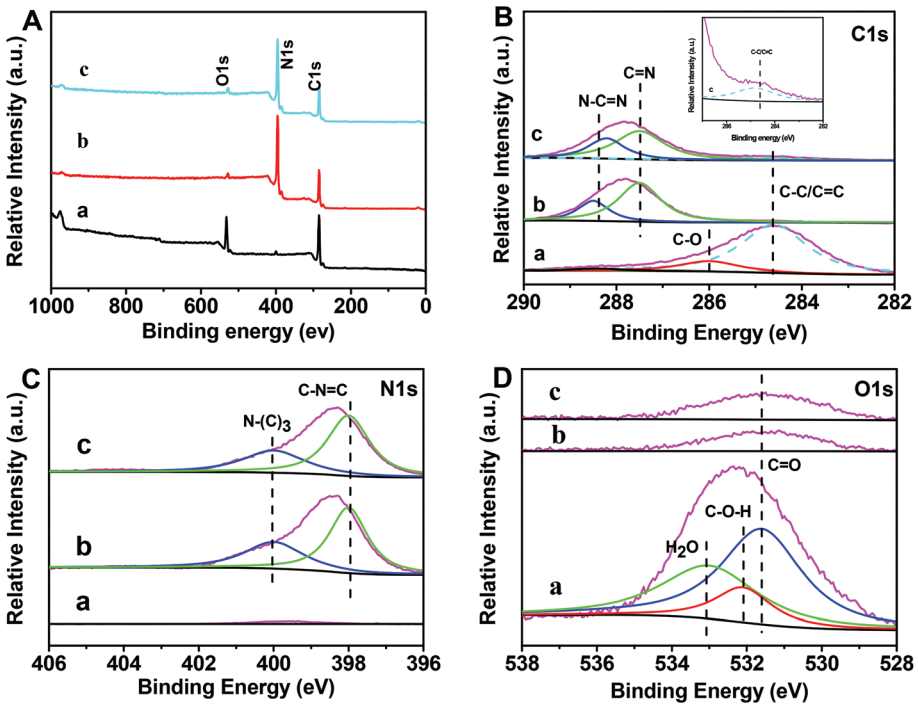

Fig. 4 The XPS survey spectra (A) and high-resolution XPS spectra of (B) C 1s, (C) N 1s and (D) O 1s for the various samples: (a) CDs, (b) g-C_3N_4, and (c) CDs/g-C_3N_4 (10 wt%).

which suggests that the amount of carbon dots was very low. From the inset in Fig. 4B-c, a weak peak at 284.7 eV corresponding to C═C was found in CDs/g-C_3N_4 (10 wt%), which suggests that the carbon dots were successfully introduced to the g-C_3N_4. Furthermore, the content (at%) of C, N, and O, as well as the atomic ratio of C to N (C/N) for the samples were calculated using the XPS analysis and are listed in Table 1. It was found that the C/N ratio for g-C_3N_4 and CDs/g-C_3N_4 was 0.67 and 0.73, respectively. The increase in the C/N ratio also proves the successful modification of the carbon dots on the g-C_3N_4 sample.

In Fig. 5, the FTIR spectra further exhibit the corresponding functional groups of the carbon dots, g-C_3N_4, and CDs/g-C_3N_4. For the carbon dots, the main characteristic absorption peaks are positioned at *ca.* 786, 1023, 1384, 1621, 1704, 2868, 2970, and 3419 cm^{-1}, which can be assigned to functional groups such as C–O, C–O, –CH_3, C═C, C═O, –CH_2, –CH_3 and –OH, respectively.[46] Compared with the carbon dots, g-C_3N_4 shows different absorption peaks, which correspond to the functional groups of the tri-*s*-triazine structure (808 cm^{-1}), heptazine heterocycles (1635, 1410 and 1242 cm^{-1}) and the unreacted amino group (3100–3300 cm^{-1}).[21] Similar to the XPS spectra, the CDs/g-C_3N_4 also exhibits a similar FTIR spectrum with g-C_3N_4 due to (i) the small amount of carbon dots in CDs/g-C_3N_4 and (ii) the overlap of peak positions such as C═C in the carbon dots and the heptazine heterocycles in g-C_3N_4. The g-C_3N_4 modified with carbon dots can also be demonstrated by the UV-vis spectra and digital photographs shown in Fig. 6. It is clear that g-C_3N_4 exhibits a strong band-edge absorption at *ca.* 420 nm. In comparison, the CDs/g-C_3N_4 samples show a red-shift in the absorption edge and an additional shoulder peak from 450 to 600 nm compared with g-C_3N_4. Furthermore, the intensities of the shoulder peak

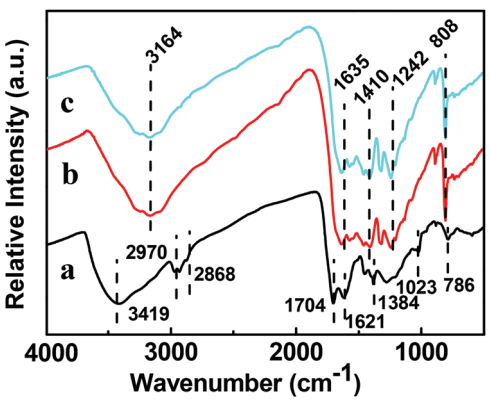

Fig. 5 The FTIR spectra of the various samples: (a) CDS; (b) g-C_3N_4 and (c) CDs/g-C_3N_4 (10 wt%).

Table 1 The content (at%) of the various elements determined using XPS: (A) CDs; (B) g-C_3N_4 and (C) CDs/g-C_3N_4 (10 wt%)

Sample	C	N	O	C/N
A	77.58	2.57	19.85	30.19
B	39.37	58.53	2.1	0.67
C	41.09	56.23	2.68	0.73

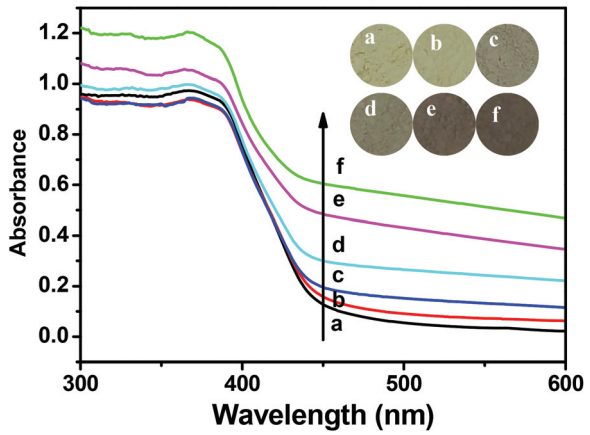

Fig. 6 The UV-vis spectra and photographs (inset) of the various samples: (a) g-C_3N_4, (b) CDs/g-C_3N_4 (1 wt%), (c) CDs/g-C_3N_4 (5 wt%), (d) CDs/g-C_3N_4 (10 wt%), (e) CDs/g-C_3N_4 (50 wt%) and (f) CDs/g-C_3N_4 (100 wt%).

gradually increase with an increase in the amount of carbon dots in CDs/g-C_3N_4. The shoulder peak is mainly caused due to the light absorption of carbon dots, and the red-shift in the absorption edge suggests the interfacial interactions between the CDs and g-C_3N_4. In addition, the digital photographs show that the colours of the CDs/g-C_3N_4 samples change from pale yellow to dark brown upon increasing the amount of carbon dots (inset in Fig. 6), which also indicates that the carbon dots have been successfully modified on the surface of their corresponding samples. On the basis of the above results, such as SEM, TEM, XRD, XPS, FTIR and UV-vis spectra, it was clearly demonstrated that the carbon dots have been homogeneously and solidly modified on the surface of g-C_3N_4 to form the CDs/g-C_3N_4 photocatalysts using a facile hydrothermal approach.

Photocatalytic performance and mechanism

The photocatalytic performance of the CDs/g-C_3N_4 photocatalysts with different amounts of carbon dots was evaluated using the photocatalytic H_2-evolution reaction with a lactic acid aqueous solution (10 vol%) used as the sacrificial agent. The corresponding results are shown in Fig. 7A. It can be seen that all of the CDs/g-C_3N_4 photocatalysts exhibit a higher H_2 production than g-C_3N_4. More specifically, the CDs/g-C_3N_4 (10 wt%) sample shows the highest H_2 production (*ca.* 2.2 μmol h^{-1}), which is *ca.* 4.4 times more than that found for g-C_3N_4 (*ca.* 0.5 μmol h^{-1}). The enhanced photocatalytic performance of CDs/g-C_3N_4 may originate from (i) a rapid photogenerated electron transfer from the LUMO of g-C_3N_4 to the LUMO of the carbon dots and (ii) the increased number of active sites provided by the carbon dots (Fig. 8A). Subsequently, the CDs/g-C_3N_4 photocatalysts were further modified using a Pt co-catalyst *via* a photoreduction approach and the photocatalytic performance of the corresponding samples were evaluated under the same conditions as described in the above tests. The metallic Pt nanoparticles in CDs/g-C_3N_4 (100 wt%) were characterized using TEM (Fig. S2a and b†). The

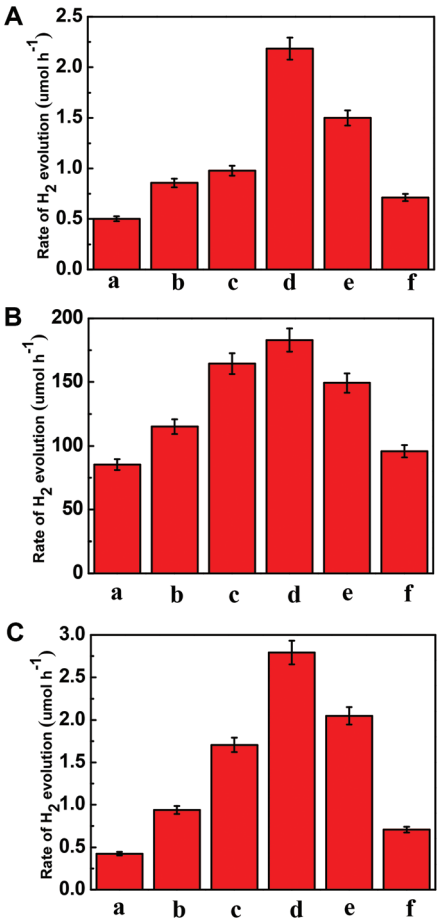

Fig. 7 The photocatalytic H_2-evolution rate of (a) g-C_3N_4, (b) CDs/g-C_3N_4 (1 wt%), (c) CDs/g-C_3N_4 (5 wt%), (d) CDs/g-C_3N_4 (10 wt%), (e) CDs/g-C_3N_4 (50 wt%) and (f) CDs/g-C_3N_4 (100 wt%) with (A) lactic acid as the sacrificial agent, (B) lactic acid as the sacrificial agent and an additional Pt co-catalyst, and (C) pure water and an additional Pt co-catalyst.

Pt nanoparticles with a uniform diameter of *ca.* 2 nm were homogeneously distributed on the surface of the carbon dots or g-C_3N_4. As shown in Fig. 7B, upon loading the Pt co-catalysts, the amount of H_2 production for the Pt-CDs/g-C_3N_4 samples was significantly increased compared with their corresponding CDs/g-C_3N_4 samples. Furthermore, Pt-CDs/g-C_3N_4 (10 wt%) also showed the highest H_2 production (*ca.* 183.0 μmol h^{-1}), which was *ca.* 2.1 times more than found for Pt/g-C_3N_4 (*ca.* 85.4 μmol h^{-1}). Furthermore, the photocatalytic performance of the Pt-CDs/g-C_3N_4 photocatalysts was also evaluated under visible-light irradiation (λ = 420 nm) using lactic acid as the sacrificial agent. The corresponding results are shown in Fig. S2† and exhibit a similar trend with those tested under UV-light irradiation. Therein, all of the CDs/g-C_3N_4 photocatalysts exhibit higher H_2 production than g-C_3N_4. Similarly, Pt-CDs/g-C_3N_4 (10 wt%) shows the highest H_2 production (*ca.* 48.1 μmol h^{-1}). However, the rates of H_2 evolution for the samples are lower under visible-light irradiation (λ = 420 nm) than under UV-light irradiation (λ = 365 nm). Clearly,

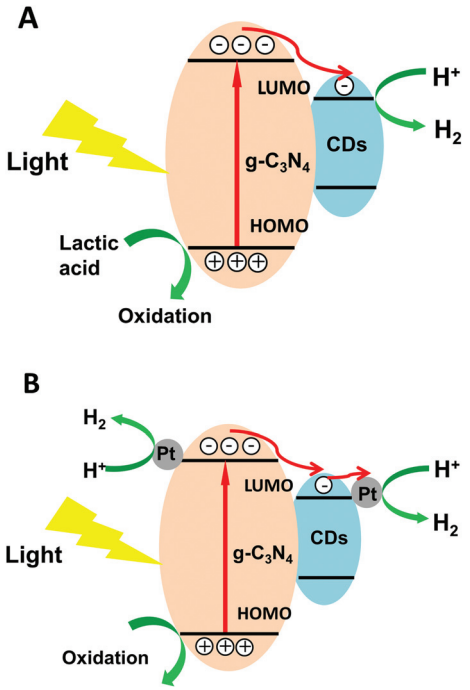

Fig. 8 Schematic of the photocatalytic H_2-evolution mechanisms for the (A) CDs/g-C_3N_4 and (B) Pt-CDs/g-C_3N_4.

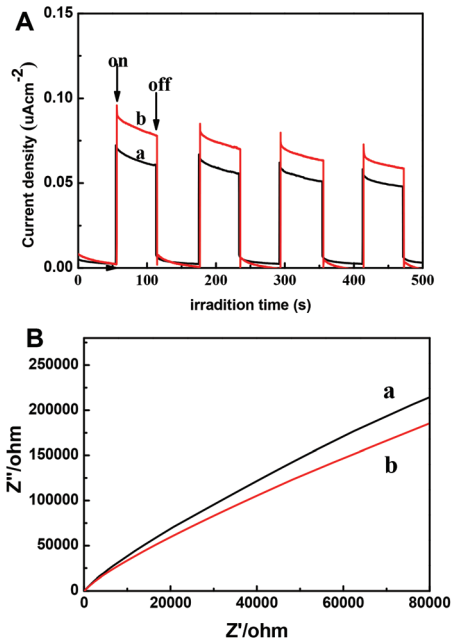

Fig. 9 The (A) transient photocurrent responses and (B) electrochemical impedance spectra of (a) g-C_3N_4 and (b) CDs/g-C_3N_4 (10 wt%).

the carbon dots play an important role in the improvement of the photocatalytic H_2 production in the Pt-CDs/g-C_3N_4 samples. According to the photocatalytic mechanism shown in Fig. 8B, the carbon dots can promote the effective transfer of photogenerated electrons from the LUMO of g-C_3N_4 to the LUMO of the carbon dots as electron mediators. Then, the photogenerated electrons are transferred from the carbon dots to the metallic Pt co-catalyst due to its high electrical conductivity. Finally, the H_2O molecules are rapidly reduced to H_2 by the photogenerated electrons on the Pt co-catalyst due to their excellent active sites and low overpotential. Therefore, the improved H_2-evolution performance of Pt-CDs/g-C_3N_4 originates from the rapid interfacial charge transfer and catalytic reaction, similar to our recent Fe(III)-rGO/TiO_2 photocatalyst.[47,48] In addition, the Pt-CDs/g-C_3N_4 photocatalysts can even split pure water to produce H_2 due to their outstanding photocatalytic reduction properties. From Fig. 7C, it is seen that Pt-CDs/g-C_3N_4 (10 wt%) show the optimum photocatalytic performance for H_2 production and the rate was *ca.* 2.8 μmol h^{-1}. However, the amount of O_2 evolution was not detected in the cases, which can be attributed to the dissolution of O_2 in water or the formation of other oxidation productions (H_2O_2, *etc.*).[43,49]

To further demonstrate the rapid transfer of photogenerated electrons from g-C_3N_4 to the carbon dots, the photoelectrochemical (PEC) analysis of CDs/g-C_3N_4 (10 wt%) was employed, which is a powerful technique used to study the interfacial charge transfer and recombination rates.[39] The transient photocurrent–time (*i*–*t*) curves obtained for g-C_3N_4 and CDs/g-C_3N_4 (10 wt%) under intermittent visible-light irradiation (λ > 300 nm) are shown in Fig. 9A. It is clear that the photocurrent of CDs/g-C_3N_4 (10 wt%) was higher than that observed for g-C_3N_4, indicating that the carbon dots can efficiently boost the interfacial charge transfer. Furthermore, it can also be seen that the arc radius of the EIS plots for CDs/g-C_3N_4 (10 wt%) was smaller than that observed for g-C_3N_4 under light irradiation (Fig. 9B), suggesting a smaller charge transfer resistance on the electrode surface for CDs/g-C_3N_4, indicating the higher efficiency of photoinduced electron–hole pairs through an interfacial interaction between g-C_3N_4 and the carbon dots.

Conclusions

To summarize, a facile hydrothermal approach was developed to prepare CDs/g-C_3N_4 photocatalysts using L-ascorbic acid and g-C_3N_4 as precursors. Upon the *in situ* thermal polymerization of L-ascorbic acid on the surface of g-C_3N_4, the carbon dots were homogeneously and solidly modified on the g-C_3N_4 surface. The CDs/g-C_3N_4 photocatalysts showed a higher photocatalytic performance for H_2 production than g-C_3N_4 under UV light irradiation. The improved photocatalytic performance of CDs/g-C_3N_4 mainly originates from rapid interfacial charge transfer. After a Pt co-catalyst was loaded onto the as-prepared sample, the Pt-CDs/g-C_3N_4 photocatalyst formed exhibited excellent photocatalytic performance for H_2 production and could even split pure water to produce H_2. Considering our present economic and facile synthetic approach for the modification of carbon dots on the surface of g-C_3N_4 photocatalysts, the as-prepared CDs/g-C_3N_4 photocatalysts will be promising for practical use in water splitting.

Acknowledgements

This study was supported by the National Natural Science Foundation of China (51672203, 51472192 and 21477094). This study was also financially supported by the Fundamental Research Funds for the Central Universities (WUT 2017IB002).

Notes and references

1 X. Wang, K. Maeda, A. Thomas, K. Takanabe, G. Xin, J. M. Carlsson, K. Domen and M. Antonietti, *Nat. Mater.*, 2009, **8**, 76.
2 S. Cao and J. Yu, *J. Phys. Chem. Lett.*, 2014, **5**, 2101.
3 G. Dong, K. Zhao and L. Zhang, *Chem. Commun.*, 2012, **48**, 6178.
4 C. Ye, J. X. Li, Z. J. Li, X. B. Li, X. B. Fan, L. P. Zhang, B. Chen, C. H. Tung and L. Z. Wu, *ACS Catal.*, 2015, **5**, 6973.
5 H. Yu, F. Chen, F. Chen and X. Wang, *Appl. Surf. Sci.*, 2015, **358**, 385.
6 Y. Xu, M. Xie, S. Huang, H. Xu, H. Ji, J. Xia, Y. Li and H. Li, *RSC Adv.*, 2015, **5**, 26281.
7 P. Li, W. Zhang, Y. Zhang, Y. Sun and F. Dong, *RSC Adv.*, 2016, **6**, 96334.
8 M. Tahir, N. Mahmood, L. Pan, Z. F. Huang, Z. Lv, J. Zhang, F. K. Butt, G. Shen, X. Zhang, S. X. Dou and J. J. Zou, *J. Mater. Chem. A*, 2016, **4**, 12940.
9 W. J. Ong, L. L. Tan, Y. H. Ng, S. T. Yong and S. P. Chai, *Chem. Rev.*, 2016, **116**, 7159.
10 L. Lin, H. Ou, Y. Zhang and X. Wang, *ACS Catal.*, 2016, **6**, 3921.
11 Y. Li, J. Zhan, L. Huang, H. Xu, H. Li, R. Zhang and S. Wu, *RSC Adv.*, 2014, **4**, 11831.
12 D. Peng, H. Wang, K. Yu, Y. Chang, X. Ma and S. Dong, *RSC Adv.*, 2016, **6**, 77760.
13 S. Zhang, J. Li, M. Zeng, J. Xu, X. Wang and W. Hu, *Nanoscale*, 2014, **6**, 4157.
14 J. Ran, T. Y. Ma, G. Gao, X. W. Du and S. Z. Qiao, *Energy Environ. Sci.*, 2015, **8**, 3708.
15 G. Dong, K. Zhao and L. Zhang, *Chem. Commun.*, 2012, **48**, 6178.
16 G. Zhang, Z. A. Lan, L. Lin, S. Lin and X. Wang, *Chem. Sci.*, 2016, **7**, 3062.
17 S. Ma, S. Zhan, Y. Jia, Q. Shi and Q. Zhou, *Appl. Catal., B*, 2016, **186**, 77.
18 J. Xue, S. Ma, Y. Zhou, Z. Zhang and M. He, *ACS Appl. Mater. Interfaces*, 2015, **7**, 9630.
19 X. Wei, C. Shao, X. Li, N. Lu, K. Wang, Z. Zhang and Y. Liu, *Nanoscale*, 2016, **8**, 11034.
20 G. Dong, L. Yang, F. Wang, L. Zang and C. Wang, *ACS Catal.*, 2016, **6**, 6511.
21 X. C. Wang, S. Blechert and M. Antonietti, *ACS Catal.*, 2012, **2**, 1596.
22 Q. Sun, P. Wang, H. Yu and X. Wang, *J. Mol. Catal. A: Chem.*, 2016, **424**, 369.
23 Z. Tong, D. Yang, J. Shi, Y. Nan, Y. Sun and Z. Jiang, *ACS Appl. Mater. Interfaces*, 2015, **7**, 25693.
24 W. Wan, S. Yu, F. Dong, Q. Zhang and Y. Zhou, *J. Mater. Chem. A*, 2016, **4**, 7823.
25 J. Liu, H. Xu, Y. Xu, Y. Song, J. Lian, Y. Zhao, L. Wang, L. Huang, H. Ji and H. Li, *Appl. Catal., B*, 2017, **207**, 429.
26 J. Liu, Y. Zhang, L. Lu, G. Wu and W. Chen, *Chem. Commun.*, 2012, **48**, 8826.
27 G. Gao, Y. Jiao, F. Ma, Y. Jiao, E. Waclawik and A. Du, *Phys. Chem. Chem. Phys.*, 2015, **17**, 31140.
28 Y. Hou, A. B. Laursen, J. Zhang, G. Zhang, Y. Zhu, X. Wang, S. Dahl and I. Chorkendorff, *Angew. Chem., Int. Ed.*, 2013, **52**, 3621.
29 H. Li, Z. Kang, Y. Liu and S. T. Lee, *J. Mater. Chem.*, 2012, **22**, 24230.
30 F. Wang, M. Kreiter, B. He, S. Pang and C. Y. Liu, *Chem. Commun.*, 2010, **46**, 3309.
31 Z. Ma, R. Sa, Q. Li and K. Wu, *Phys. Chem. Chem. Phys.*, 2016, **18**, 1050.
32 H. Zhang, L. Zhao, F. Geng, L. H. Guo, B. Wan and Y. Yang, *Appl. Catal., B*, 2016, **180**, 656.
33 S. Fang, Y. Xia, K. Lv, Q. Li, J. Sun and M. Li, *Appl. Catal., B*, 2016, **185**, 225.
34 H. Sun, G. Zhou, Y. Wang, A. Suvorova and S. Wang, *ACS Appl. Mater. Interfaces*, 2014, **6**, 16745.
35 X. Xia, N. Deng, G. Cui, J. Xie, X. Shi, Y. Zhao, Q. Wang, W. Wang and B. Tang, *Chem. Commun.*, 2015, **51**, 10899.
36 X. Jian, X. Liu, H. Yang, J. Li, X. Song, H. Dai and Z. Liang, *Appl. Surf. Sci.*, 2016, **370**, 514.
37 Z. F. Huang, J. Song, L. Pan, Z. Wang, X. Zhang, J. J. Zou, W. Mi, X. Zhang and L. Wang, *Nano Energy*, 2015, **12**, 646.
38 H. Yu, X. Huang, P. Wang and J. Yu, *J. Phys. Chem. C*, 2016, **120**, 3722.
39 P. Wang, Y. Lu, X. Wang and H. Yu, *Appl. Surf. Sci.*, 2017, **391**, 259.
40 F. Chen, H. Yang, X. Wang and H. Yu, *Chin. J. Catal.*, 2017, **38**, 296.
41 B. Zhang, C. Y. Liu and Y. Liu, *Eur. J. Inorg. Chem.*, 2010, **2010**, 4411.
42 L. R. Zou, G. F. Huang, D. F. Li, J. H. Liu, A. L. Pan and W. Q. Huang, *RSC Adv.*, 2016, **6**, 86688.
43 H. Ming, Z. Ma, Y. Liu, K. Pan, H. Yu, F. Wang and Z. Kang, *Dalton Trans.*, 2012, **41**, 9526.
44 H. Yu, P. Xiao, P. Wang and J. Yu, *Appl. Catal., B*, 2016, **193**, 217.
45 Q. L. Zhao, Z. L. Zhang, B. H. Huang, J. Peng, M. Zhang and D. W. Pang, *Chem. Commun.*, 2008, **12**, 5116.
46 J. Wang, M. Gao and G. W. Ho, *J. Mater. Chem. A*, 2014, **2**, 5703.
47 H. Yu, J. Tian, F. Chen, P. Wang and X. Wang, *Sci. Rep.*, 2015, **5**, 13083.
48 Y. Xu, Y. Mo, J. Tian, P. Wang, H. Yu and J. Yu, *Appl. Catal., B*, 2016, **181**, 810.
49 J. Liu, Y. Liu, N. Liu, Y. Han, X. Zhang, H. Huang, Y. Lifshitz, S. T. Lee, J. Zhong and Z. Kang, *Science*, 2015, **347**, 970.

